UNICA UNIVERSITÀ DEGLI STUDI DI CAGLIARI

This is the Author's [*accepted*] manuscript version of the following contribution:

Elio Fiorito, Fantauzzi Marzia, Brundu Laura, Atzei Davide, Elsener Bernhard, Rossi Antonella.

Spectroscopic evidence for clarifying the mechanism of toxic element removal by marble waste

Vacuum, 196, February 2022, paper n. 110721

The publisher's version is available at:

http:// 10.1016/j.vacuum.2021.110721

When citing, please refer to the published version.

This full text was downloaded from UNICA IRIS https://iris.unica.it/

Spectroscopic evidence for clarifying the mechanism of toxic element removal by marble waste.

Elio Fiorito [a], Marzia Fantauzzi [a, *], Laura Brundu [a], Davide Atzei [a], Bernhard Elsener [a], Antonella Rossi [a *]

Affiliation:

[a] Department of Chemical and Geological Sciences, University of Cagliari, Campus of Monserrato (CA), I-09042 Monserrato, Italy

***Corresponding Authors:**

Prof. Marzia Fantauzzi, Department of Chemical and Geological Sciences, Università di Cagliari, I-09042 Monserrato (CA), Italy. Tel: +39 070/675-4464; email: fantauzzi@unica.it

Prof. Antonella Rossi, Department of Chemical and Geological Sciences, Università di Cagliari, I-09042 Monserrato (CA), Italy. Tel: +39 070/675-4464; email: rossi@unica.it

Abstract

Powdered marble waste (MW) resulting from cutting processes in Orosei marble district is tested as sorbent for toxic elements from wastewater in compliance with European circular economy strategy. MW consists of calcite polymorph of $CaCO_3$ with a Mg content of about 0.28 wt%. This article focuses on the use of surface analyses of MW as sorbent by X-ray photoelectron spectroscopy (XPS) and solution analyses by ICP-AES for distinguishing between the different removal mechanisms of Pb^{2+} and Mn^{2+} from model solutions in a wide concentration range, from 0.1 μM to 100 mM. The results showed a removal efficiency (RE) of about 100% for Pb independently from the initial concentration and up to about 100% for manganese, when its initial

concentration is lower than 0.1 mM. These findings help in the development of remedial actions and analytical strategies for water remediation.

Keywords: Marble waste powder, X-ray photoelectron spectroscopy (XPS), Induced coupled plasma atomic emission spectroscopy (ICP AES), surface reactivity, lead, manganese

Mining activity at Orosei's marble district (North-East Sardinia, Italy) produces a significant amount of waste material, e.g. in 2018 249 tons of waste was produced in that area [1]. These "wastes resulting from exploration, mining, dressing and further treatment of minerals and quarry" (European Waste Catalogue [2]) should be considered as a resource to re-use in accordance with waste hierarchy principle (prevention, preparing for reuse, recycling, other recovery and disposal) in the framework of the Circular Economy Strategy (EU COM/2015/0614) [3]. Such an application could be the treatment of polluted water and wastewater. In this project, marble waste powder is used as sorbent for Pb^{2+} and Mn^{2+} in model solutions, for evaluating the removal efficiency of toxic elements from water and to clarify the removal mechanism. XPS surface analysis was used for the characterization of the marble waste (MW) before and after sorption tests, while inductively coupled plasma – atomic emission spectroscopy (ICP-AES) was exploited for solutions analysis.

Samples of powder resulting from the cutting process of marble blocks were collected from marble quarry located in Orosei (Latitude: 40°21'34.4" N; Longitude: 9°40'10.9" E; north-eastern Sardinia, Italy) in collaboration with BS QuarrySar Group, XRD analyses on marble waste showed that it only consists of calcite polymorph with a Mg content of about 0.28 wt% and an average particle size of 5 (2) μm. The sorption tests were performed under atmospheric conditions in a closed vessel in order to avoid the influence of the environmental CO_2, which might dissolve in the solution. 0.5000 g of marble waste was suspended in 0.05 dm^3 of Pb^{2+} or Mn^{2+} solutions for 24 hours at T=293.15 K. $Pb(NO_3)_2$ was used to prepare solutions of Pb^{2+} with initial concentrations in the range 0.1 μM – 80 mM. The pH of the Pb^{2+} model solutions decreased with the increase of Pb^{2+} concentration and it ranged between 6.85 (0.02) and 4.2 (0.1).. $Mn(NO_3)_2{\cdot}4H_2O$ was employed for Mn^{2+} - containing solutions with initial concentrations ranging between 0.1 μM and 100 mM. Also in this case, the pH of the solutions depended on Mn^{2+} concentration and it ranged between 5.54 (0.06) and 4.22 (0.03). After the removal experiments the solution was filtered and the powder

collected on the filter was washed with double-distilled water dried in oven (T = 383.15 K) for 24 hours and then stored in Eppendorf tubes before the XPS analysis.

A Theta Probe XP-spectrometer (Thermo Fisher Scientific, East Grinstead, UK) was used for surface analyses. The powders were pressed as pellets and the spectra were recorded irradiating the surface with a monochromatic Al kα X-ray source (Al $k\alpha_{1,2}$ = 1486.6 eV). The analysed area was estimated to be 0.5 mm^2 [4] Spectra were acquired in fixed analyzer transmission mode (FAT) and the pass energy was set at 200 and at 120 eV for survey and high-resolution spectra, respectively. A flood gun was used for charge neutralization. The residual pressure during analyses was lower than $2x10^{-5}$ Pa due to the utilization of low energy argon ions for charge neutralization. The spectrometer was calibrated according to ISO 15472:2014. Three different areas on each pressed pellet were analysed. All binding energies were referred to C 1s signal at 285.0 eV. Casa XPS software (2.3.19PR1.0 version, Ltd., UK) was used for spectra processing. The background was subtracted according to the Tougaard routine [5]. The spectra were curve fitted using asymmetric line-shapes based on the Lorentzian functional form convoluted with a Gaussian one [6]. Surface composition was calculated based on the peak areas corrected for calculated sensitivity factors; more details on are provided in [7].

Solution analyses before and after contact with the model solutions were performed by Agilent 5110 (ICP-AES) spectrophotometer. Ion removal efficiency (RE%) was calculated from solution analyses results, by the formula: $R.E.\% = [(C_i - C_f) / C_i] \times 100$ where C_i and C_f are the initial and final concentration of Pb^{2+} or Mn^{2+}.

XPS spectra were exploited to obtain information on the chemical state of the elements and to calculate the surface composition of the powder samples before and after sorption tests. The high-resolution spectra of Pb 4f (Fig. 1a) indicate that lead is not detected on the sample surface following sorption tests in solutions with Pb^{2+} concentration below 0.01 mM. The binding energy (BE) of Pb $4f_{7/2}$ was found to be at 139.1 (0.2) eV and it is in agreement with the BE value observed

on a commercial $PbCO_3$ used as reference material. Manganese, Mn 2p spectra (Fig. 1b), was not detected when the concentration of Mn^{2+} - solutions was lower than 0.1 mM. The Mn $2p_{3/2}$ peak (Fig. 1d) was curve-fitted taking into account the multiplet splitting in agreement with [8]. In addition an intense shake-up satellite was detected. The energy separation between the peaks and the area ratio were constrained according to results obtained on a commercial $MnCO_3$ sample analysed using the same settings. The binding energy of the first peak of the multiplet was found at 641.0 (0.2) eV. This value is typical for $MnCO_3$ in agreement with [9]

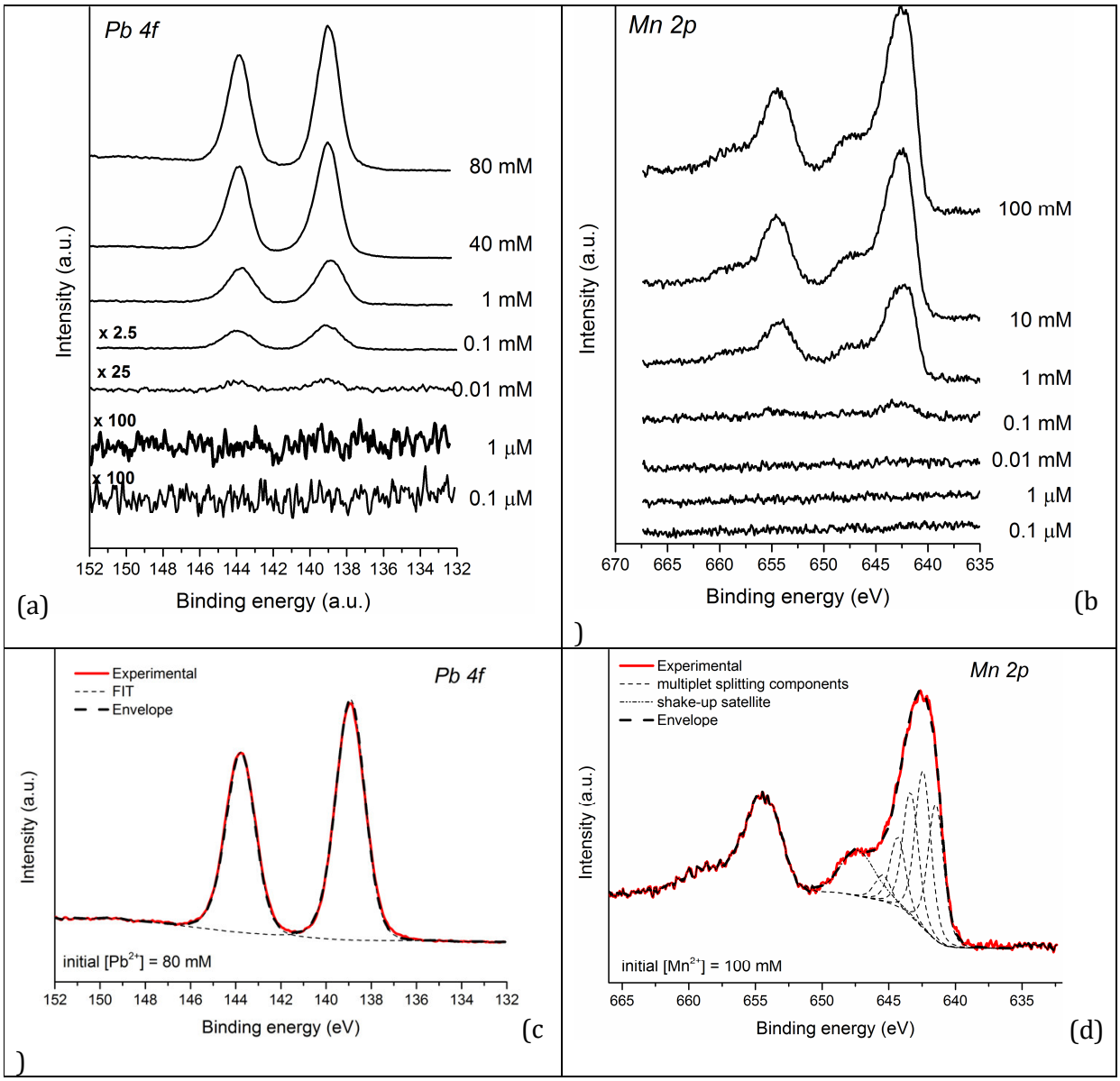

Figure 1: Pb 4f and Mn 2p XP spectra recorded on: (a) samples after Pb^{2+} sorption tests and (b) Mn^{2+} sorption tests. An example of curve fitting of (c) Pb 4f and (d) Mn $2p_{3/2}$ is provided.

Based on the area of the main photoelectron peaks (Ca, Pb, Mn, O, C) of the samples, quantitative analysis was carried out for getting an insight on the surface composition. According to stoichiometry the composition of $CaCO_3$ should be: 20% calcium, 20% carbon and 60% oxygen. The surface concentration (at%) of lead and calcium on the samples from Pb^{2+} sorption tests and of manganese and calcium on the samples from Mn^{2+} sorption tests is presented in Figure 2.

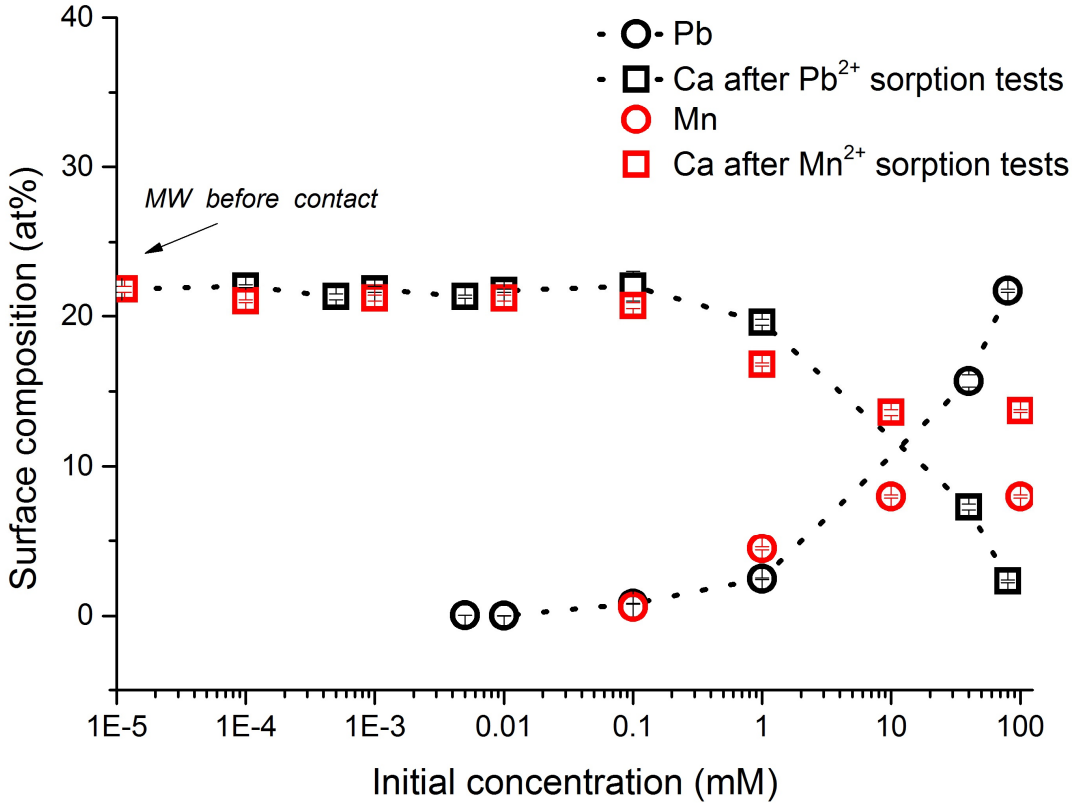

Figure 2: Surface lead, manganese and calcium concentration (at%) from XPS data, following lead and manganese sorption tests.

Calcium content on marble waste surface before the contact with the lead and manganese solutions was found to be 21 (1) at%, in very good agreement with the expected stoichiometry of $CaCO_3$ (20%). For lead sorption tests up to an initial Pb^{2+} concentration equal to 0.1 mM, the calcium concentration at the surface remains constant at 21 (1) %. The lead signal is indeed detected but this finding has to be ascribed to the fact that the analysed area by XPS is much greater than the size of

lead carbonate aciculae. Thus the composition has to be regarded as an average composition. Then a decrease in calcium and a concomitant increase in Pb concentration were revealed, the sum Ca (at%) + Pb (at%) is always about 20%. The ratios Ca (at%) + Pb (at%) / $C_{carbonate}$ (at%) and $O_{carbonate}$/ $C_{carbonate}$ (at%) (not shown) are found to be 1.2 (0.1) and 2.9 (0.1) respectively, in agreement with the expected stoichiometry of $CaCO_3$, $PbCO_3$ and of their mixture. This finding substantiates the presence of these carbonates as isolated compounds or as mixture on the MW-sorbent particles. The higher the initial concentration of lead ions in the solution the higher the amount of $PbCO_3$. When the initial Pb^{2+} solution is 80 mM, lead concentration at the surface after sorption test is found to be about 20% while Ca is barely detected. SEM-EDX analyses of the samples (not shown) allows the observation of prismatic acicular lead phases attributable to $PbCO_3$; this precipitate covers MW particles when MW is suspended in 40 mM and 80 mM Pb^{2+} solutions; XRD patterns (not shown) confirm the presence of cerussite.

When MW powder is used to remove manganese Mn^{2+} from the solution, a similar trend in calcium and manganese concentration at the surface is observed as for Pb^{2+} removal (Figure 2). Up to initial Mn^{2+} concentrations of 0.1 mM, manganese is not or only barely detected (see also Fig. 1b), at higher initial Mn^{2+} concentration the manganese on the surface increases, but even at the highest initial concentration of 100 mM of Mn^{2+}, only 7% of manganese (and 13 at% of calcium) were revealed at the surface. In contrast to the interaction of MW with lead solutions, neither SEM nor XRD on marble waste powder suspended in Mn^{2+} bearing solutions revealed the presence of precipitates.

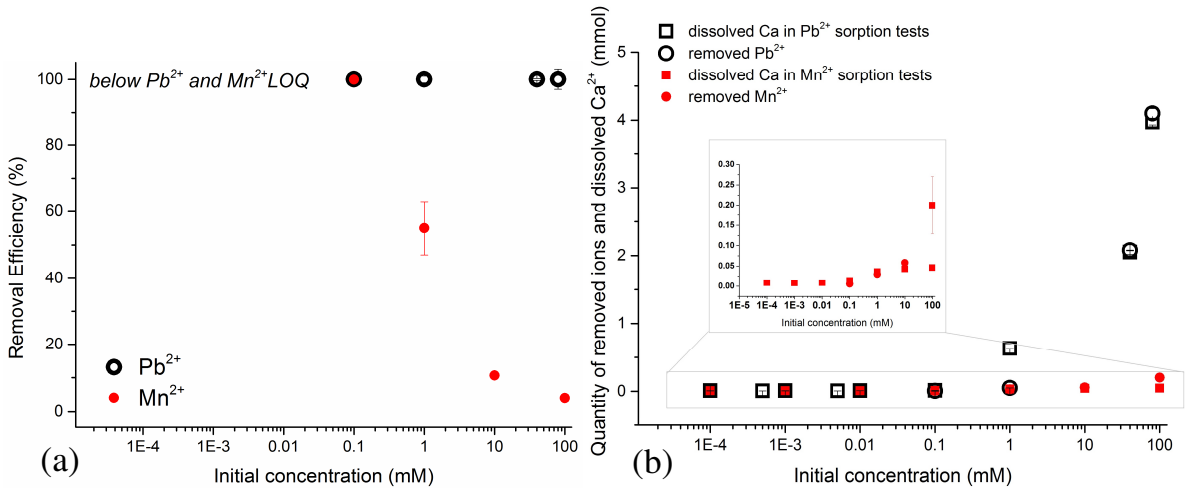

Figure 3: (a) Pb^{2+} and Mn^{2+} removal efficiency; (b) millimoles of dissolved calcium, removed lead and removed manganese in Pb^{2+} and Mn^{2+} sorption tests.

The removal efficiency for lead Pb^{2+} using marble waste (Figure 3a) is always 100% (note that a 100% removal efficiency for 50 cm^{-3} of a 80 mM Pb^{2+} solution corresponds to a quantity of 4 mmol of Pb^{2+} removed, see Fig. 3b). For concentrations lower than 0.1 mM, the amount of residual lead (and manganese) is below the limit of quantification (LOQ) beeing10 µg/dm^3 for lead and 2 µg/dm^3 for manganese, respectively. In contrast to Pb $^{2+}$, Mn^{2+} removal efficiency decreases from 99.95% for an initial concentration of 0.1 mM to only 4% when the initial concentration is of 100 mM.

The difference in the removal efficiency between Pb^{2+} and Mn^{2+} might be explained taking into account two important factors: 1) the different solubility products of the calcium-, lead- and manganese carbonates, and 2) the difference in ionic radius of calcium, lead and manganese. Among the three carbonates, $PbCO_3$ (K_{ps} = 7.4 x 10^{-14}) has by far the lowest solubility product compared to $CaCO_3$ (K_{ps} = 4.5 x 10^{-9}) and $MnCO_3$ (K_{ps} = 5.1 x 10^{-10}), thus $PbCO_3$ will precipitate and Pb^{2+} removed from the solutions. Two different phases, $PbCO_3$ (cerussite) and $(PbCO_3)_2Pb(OH)_2$ (hydrocerussite), are formed depending on the concentration of Pb^{2+} and on the pH [10]. XRD results (not shown) confirmed that only cerussite precipitated when $[Pb^{2+}] \geq 40$ mM, while both hydrocerussite and cerussite are present at lower $[Pb^{2+}]$ concentrations. This is in agreement with literature, where a decrease in pH due to the Brönsted acid behaviour of Pb^{2+}

leading to the formation of hydroxo-complexes and H^+ [11] is reported. This pH decrease determines the dissolution of calcium carbonate leading to an increase of dissolved calcium (Fig. 3b) and the precipitation of $PbCO_3$. Hydrocerussite precipitation is favoured at neutral or basic pH, thus at lower Pb^{2+} concentrations.

Regarding Mn^{2+} removal, a phase precipitation of $MnCO_3$ can be excluded as removal mechanism (and no precipitates were observed) because the suspensions of MW in Mn^{2+} solutions with initial concentrations ranging between 0.1 μM – 0.01 mM are undersaturated with respect to $MnCO_3$. Instead, manganese removal mechanism could involve ion-exchange adsorption [12] through the reaction:

$$Mn^{2+}_{(aq)} + CaCO_{3\,(s)} \rightleftarrows Ca_xMn_{1-x}CO_{3\,(s)} + (1-x)Ca^{2+}_{(aq)} + xMn^{2+}_{(aq)}$$

As the ionic radius of Mn^{2+} is smaller than Ca^{2+} (83 pm *vs* 100 pm), manganese ions can easily be incorporated into the calcite structure, resulting in a solid solution called manganoan calcite, a mineral with formula $Ca_xMn_{1-x}CO_3$. As a consequence, the amount of dissolved calcium remains very low and reaches a plateau (Figure 3b). The irreversible chemisorption with formation of $Ca_xMn_{1-x}CO_3$ on the calcite surface causes the inhibition of calcite dissolution [13]. From the surface composition found at high Mn^{2+} concentrations (Fig. 2), the factor x is determined as 0.65, resulting in the formula $Ca_{0.65}Mn_{0.35}CO_3$.

When $[Mn^{2+}]$ ranges between 0.1mM and 10 mM the solutions are supersaturated with respect to $MnCO_3$ and the (co)precipitation of rhodochrosite phase ($MnCO_3$) onto calcite surface might be responsible for the manganese removal and for the increase of dissolved calcium. When initial $[Mn^{2+}]$ is higher than10 mM even though solutions are supersaturated, the preferential sites for calcite dissolution are inhibited from manganese interaction and thus both dissolved calcium (Figure 3b) and Mn at the sample surface (Figure 2) reach a plateau.

The removal mechanisms are thus different: in the case of lead the precipitation of lead carbonate is the main one. In case of manganese the ion-exchange mechanism is proposed to be the main mechanism of the removal. This implies that the Ca-Mn at the surface is limiting the removal

efficiency of this cation when the calcium amount is no more available for the ion – exchange process.

Marble waste from Orosei quarry is a promising sorbent for lead removal from wastewater, showing 100% removal efficiency over a wide range of lead concentration. For initial Pb^{2+} concentration up to 0.01 mM (2.1 mg dm^{-3}), the residual Pb^{2+} is below method LOD (4 µg dm^{-3}) and therefore below the limits for drinking water (10 µg dm^{-3}) according to Italian laws [14]. For initial $[Pb^{2+}]$ concentration in the range from 0.1 mM to 1 mM (20.7 mg dm^{-3} - 207.2 mg dm^{-3}), the concentration of residual Pb^{2+} is lower than the legal limit for surface water (0.2 mg dm^{-3}), whereas at the highest $[Pb^{2+}]_{init}$ concentrations of 40 mM (8.289 mg dm^{-3}) or 80 mM (16.576 mg dm^{-3}), the residual Pb^{2+} concentration is above the legal limit for sewage water (0.3 mg dm^{-3}). In this case a second round of calcite treatment might allow reaching a Pb^{2+} below the limits fixed by the law.

Removal of Mn^{2+} from wastewater to reach drinking water quality can be achieved for suspensions with initial $[Mn^{2+}]$ in the range 0.1 µM – 0.1 mM where the final concentration is below the legal limit for drinking water (10 µg dm^{-3}). When the initial concentration is 1 mM or higher, the residual Mn^{2+} concentration is above the legal limit both for surface water (2 mg dm^{-3}) and sewage water (4 mg dm^{-3}). The inhibiting effect of high Mn^{2+} concentrations on calcite dissolution strongly affects the marble suitability for Mn removal from highly polluted waters.

References

1. Https://Delibere.Regione.Sardegna.It/Protected/53843/0/Def/Ref/DBR53826/
2. Https://Eur-Lex.Europa.Eu/Legal-Content/IT/TXT/?Uri=celex%3A32000D0532
3. Http://Eur-Lex.Europa.Eu/Legal-Content/EN/TXT/?Uri=CELEX:52015DC0614

4. Passiu, C., Rossi, A., Bernard, L., Paul, D., Hammond, J., Unger, W. E. S., et al. (2017). Fabrication and microscopic and spectroscopic characterization of planar, bimetallic, micro- and nanopatterned surfaces. *Langmuir* 33, 5657–5665. doi: 10.1021/acs.langmuir.7b00942

5. Tougaard, S., 1989. Practical algorithm for background subtraction. Surface Science, 216(3), 343-360. https://doi.org/10.1016/0039-6028(89)90380-4.

6. A Modified Lorentzian Lineshape (casaxps.com).

7. Elsener B., Pisu M., Fantauzzi M., Addari D., and Rossi A., Electrochemical and XPS surface analytical study on the reactivity of Ni-free stainless steel in artificial saliva, *Materials and Corrosion*, vol. 67, issue 6, pp.591 -599, June 2016; DOI:10.1002/maco.201608930

8. Biesinger, M. C., Payne, B. P., Grosvenor, A. P., Lau, L. W., Gerson, A. R., & Smart, R. S. C., 2011. Resolving surface chemical states in XPS analysis of first row transition metals, oxides and hydroxides: Cr, Mn, Fe, Co and Ni. Applied Surface Science, 257(7), 2717-2730. https://doi.org/10.1016/j.apsusc.2010.10.051

9. Xu, M., Riechers, S. L., Ilton, E. S., Du, Y., Kovarik, L., Varga, T., Arey, B. W., Qafoku, O., & Kerisit, S., 2017. Manganese-calcium intermixing facilitates heteroepitaxial growth at the 1014 calcite-water interface. Chemical Geology, 470, 152-163. https://doi.org/10.1016/j.chemgeo.2017.09.001

10. Davis, A. D., Webb, C. J., Sorensen, J. L., Dixon, D. J., & Hudson, R., 2018. Geochemical thermodynamics of lead removal from water with limestone. Water, Air, & Soil Pollution, 229, 1-7. https://doi.org/10.1007/s11270-018-3824-z

11. Powell, K. J., Brown, P. L., Byrne, R. H., Gajda, T., Hefter, G., Leuz, A. K., ... & Wanner, H., 2009. Chemical speciation of environmentally significant metals with inorganic ligands. Part 3: The Pb^{2++} OH^-, Cl^-, CO_3^{2-}, SO_4^{2-}, and PO_4^{3-} systems (IUPAC Technical Report). Pure and Applied Chemistry, 81, 2425-2476. http://dx.doi.org/10.1351/PAC-REP-09-03-05

12. Freiser Henry and Fernando Quintus. Ionic equilibria in analytical chemistry. John Wiley & Sons Inc., 605 Third Avenue, New York, N.Y., 1963. https://doi.org/10.1002/jps.2600531146

13. Vinson, M. D., Arvidson, R. S., & Luttge, A., 2007. Kinetic inhibition of calcite (1 0 4) dissolution by aqueous manganese (II). Journal of Crystal Growth, 307(1), 116-125. https://doi.org/10.1016/j.jcrysgro.2007.05.059.

14. Decreto Legislativo 3 aprile 2006, n. 152 and Decreto Legislativo 2 febbraio 2001, n. 31

Acknowledgements

This research has been supported by the following funding programs: MIUR – National Program PON Ricerca e Innovazione 2014-2020 for the Ph.D. grant of Elio Fiorito (Consortium UniCa and UniSS); University of Cagliari (UniCA) and Fondazione di Sardegna (FdS) for the financial support – Project number CUP F72F20000240007 (2019): "Surface-tailored Materials for Sustainable Environmental Applications"
The authors would like to thank G.E. Porcedda at the Group of Surface Analysis of the University of Cagliari.